

Start-up Stage with Improved resolution for an Electric Field Assisted Fused Deposition

Xu Ruihan^{a,b}, Bao Weijie^{a,b}, Wang Zhihai^{a,b}, Wang Yaohong^c

Abstract - Electric field assisted Fused Deposition Modeling (E-FDM) is a promising technique in the field of 3D printing. This paper studies the start-up stage of the printing, which is a process of liquid gradually deforming and making an initial contact to the substrate under the action of electric stress. Polycaprolactone (PCL), a popular material for bio-medicine, is selected as the printing material. With a home-build E-FDM system, the nozzle substrate distance, the nozzle and substrate temperatures are all holding steady. With a photography system, the process of meniscus deformation is recorded. And by image processing methods, the meniscus length and the volume of liquid at the nozzle can be obtained. At a set of initial liquid volumes (V_i), nozzle voltage is ramped to a fixed value at a fixed rate. The effects of V_i on the meniscus deformation during the start-up stage of the printing are examined. For sufficiently small V_i , the meniscus deforms into a conical (Taylor cone) shape, and a fine jet with a diameter much smaller than the nozzle diameter appears. For sufficiently large V_i , the meniscus exhibits a spindle shape when it touches the substrate. At an intermediate V_i , the Taylor cone is formed, tending to eject the fine jet. After a short period of stagnation or even a slight retraction, no liquid is emitted. Through this study, it is suggested that for high resolution printing, ramping the voltage at small V_i may be preferable. This proposition is preliminarily confirmed in a direct writing test.

1. INTRODUCTION

Fused deposition modeling (FDM), is well-developed and maybe one of the most commonly used additive manufacturing technology¹. It is to melt the thermoplastic material in a melting chamber, extrude the molten material from the nozzle by means of air pressure or continuous feeding, and deposit the melt material layer by layer to form 3D articles. In addition to general rapid prototyping, FDM is also used in scientific researches. For example, FDM is widely employed in bio-printing, with applications in the fields of tissue engineering² and drug development³. In addition, FDM has also been used in the fabrication of microscale structures, such as microfluidic chips⁴. The advantages of the FDM method include low cost, relatively simple printing process, and compatibility with a variety of materials. However, its printing resolution is limited by the nozzle diameter. Improving printing resolution by reducing nozzle diameter faces difficulties⁵.

Electrohydrodynamic (EHD) method is popular in the field of micro-fabrication⁶. With a high voltage applied between the nozzle and a substrate, strong electric field is established at the nozzle, and the meniscus at the nozzle forms a conical shape (referred as Taylor cone) under the action of the electric stress⁷. Electrospinning is an example use of the EHD method. A fine jet, typically much thinner than the nozzle diameter, can be ejected from the end tip of the Taylor cone, and can produce micron or even nanometer diameter thin wires⁸. Electrospinning has been exploited in the field of bio-medicine, to fabricate scaffold for tissue engineering⁹. However, for the traditional electrospinning, the jet whips laterally as it is far away from the nozzle, therefore high precision printing is hard to achieve¹⁰. To avoid

this problem, a near-field EHD direct writing method is proposed, where the nozzle is put sufficiently close to the substrate, so that the liquid jet reaches the substrate before the lateral instability shows up. This method, referred here as electric field-assisted FDM (E-FDM), or in some other literatures as melt electrospinning writing (MEW), has become a promising technique for improving the print resolution^{6, 11}. This technology has been used in biomedicine, functional material preparation, and printed optoelectronics¹². Beside of the application researches, how to better control the jet is an interesting topic¹². And so far, according to our literature survey, more attention has been paid to the width of scribed line, and its dependence on those main control parameters, such as voltage, plotting speed, flow rate, and nozzle-substrate distance¹²⁻¹⁴.

In this paper, however, we focus on the process in which the liquid at the nozzle gradually deforms to make the initial contact to the substrate, before the substrate starts to move. The authors believe this research topic has practical significance, as the resolution at the starting position of the printed pattern can be quite poor. A large drop of liquid at the starting position were observed in some previous publications^{13, 14}. Especially for patterns of small line spacing, this drop of liquid could have negative impacts on subsequent printing. An example of such case is shown in Fig. 8(c). For the purpose of the high-resolution printing, we propose that the liquid would contact the substrate in the form of a fine jet with diameter much smaller than the nozzle diameter. Following such initial contact, high-resolution printing may be easier to achieve. The results of our study may be helpful for applications that need strict control to the direct writing¹⁵⁻¹⁷. An example of such applications is shown in Fig. 8(a) and (b).

With a home-build E-FDM system, the nozzle substrate distance is fixed, and the nozzle and substrate temperatures are hold steady. The flow of liquid is due to hydrostatic pressure, with more details in the next section. A typical start-up procedure for an E-FDM is to start the liquid flow first. The meniscus at the nozzle is monitored by using photography and image

^a Faculty of Information, Beijing University of Technology, Beijing 100124, China.

^b Key Laboratory of Optoelectronics Technology, Beijing University of Technology, Beijing 100124, China.

^c Center for Applied Mathematics, Tianjin University, Tianjin 300072, China.

processing. The voltage starts to ramp at time t^* , with a fixed ramping rate, till set voltage (fixed) is reached. At the moment t^* , the volume of fluid at the nozzle is referred as initial volume, denoted as $V_i = V(t^*)$. Note that t^* or equivalently V_i is the only parameter changed in this study. By ramping voltage at sufficiently small V_i (at sufficiently early time t^*), the liquid meniscus eventually deforms into the Taylor cone, and a jet with diameter much smaller than the nozzle diameter emerges. By ramping voltage at sufficiently large V_i , the liquid meniscus exhibits a spindle shape when it touches the substrate. The size of the spindle is comparable to the diameter of the nozzle. Through this study, it is suggested that for high-resolution printing, ramping the voltage at sufficiently small V_i is preferable.

Polycaprolactone (PCL), as a biodegradable material, is a commonly used material in biological printing. Cell culture scaffolds made from PCL have excellent mechanical strength and biological activity¹⁸. PCL will be used in this experiment. Although PCL can be electrospun in the forms of melt or solution, the experiments in this paper use PCL melt as printing material¹⁹.

2. Experimental

2.1 Experimental setup

The experimental setup is schematically shown in Fig. 1(a). The print head consists of a nozzle, a melting chamber, and a feeding module. The nozzle is a gauge 18 stainless steel needle, with outer diameter 1.26mm, inner diameter 0.86mm, and the needle length is 6.3mm. The nozzle is attached to the melting chamber. Typical feeding method for FDM is to squeeze the PCL wire into the melting chamber through a turning gear. With this method, the PCL flow is not uniform, possibly due to the stepping effect. With a slightly modified design, better flow rate control can be realized. As shown in Fig. 1(b), a rather large melting chamber is used to replace the tiny one for the traditional FDM machine. The flow is well consistent with Poiseuille flow under the hydrostatic pressure. By a turning gear, the PCL thin wire is fed into the melting chamber, to keep the melt level steady, either manually or automatically through machine vision monitoring. The print head is attached to a z-axis stage (Model: KSA150-11-z, from Zolix Instruments Co.). The substrate is made of 7075 Aluminum alloy, which is mounted on a translation stage that moves in the XY directions (Model: KSA150-11-x, from Zolix Instruments Co.). The substrate is heated by a heating ceramics, and the temperature can be tuned up to 200°C. The nozzle and the substrate are respectively connected to the output and the ground pole of a high-voltage power supply (Model: DW-P503-1ACDF, from Dongwen High-voltage Power Supply Co., Tianjin), with output voltage range 0-50kV, and maximum output current up to 1mA.

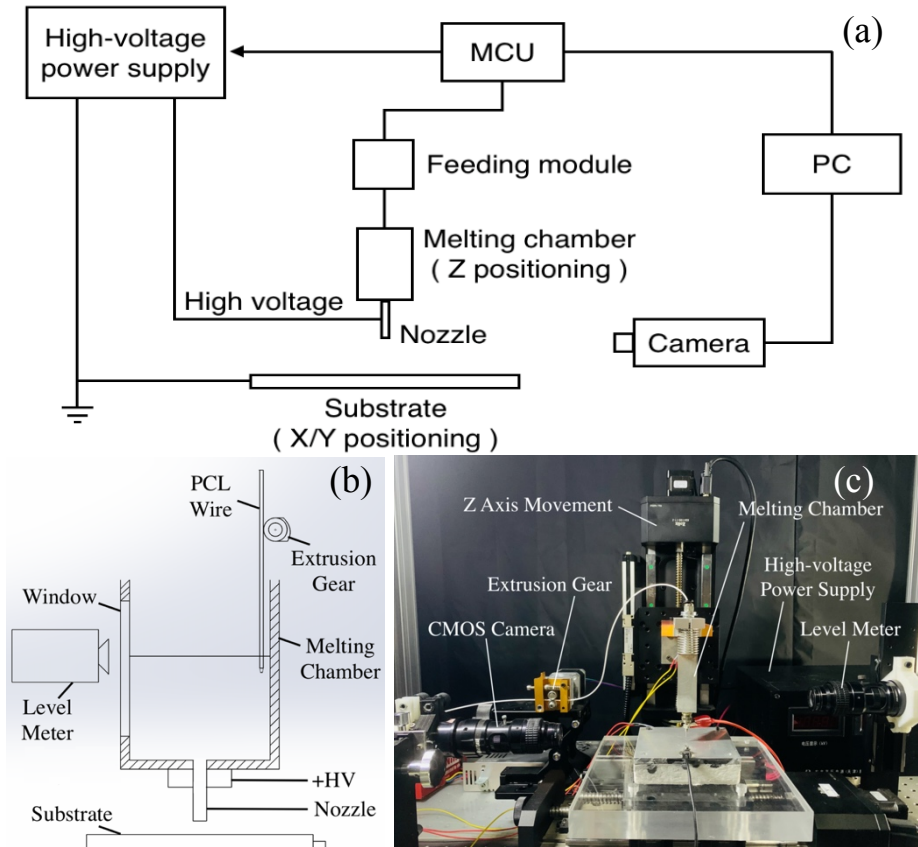


Fig. 1 (a) Schematic diagram of electric field-assisted fused deposition modelling (E-FDM) system, (b) Schematic diagram of the print head and substrate, (c) Photo of the real experimental setup

The photography system is mainly composed of a high-brightness LED and a CMOS camera. The purpose of the system is to monitor the process of the meniscus deformation. Photography is done by using a back-lightening configuration, with the nozzle staying between the LED and the camera. As shown in Fig. 2(a), the high-voltage power supply, the feeding module, the xyz positioning, and the CMOS camera are all controlled by a microcontroller (STM32) and a PC. A photo of the real instrument is shown in Fig. 1(c).

2.2 Experimental method

The morphological change of the liquid meniscus at the nozzle is obtained by the photography with the CMOS camera. The frame rate is 1 frame every 5 second, and the exposure time is 5ms. The original images are sequentially processed by an image processing software package (based on Python). First, convert the picture to grayscale, then use the Canny edge detection algorithm to extract the contour information in the picture. The Canny edge detection algorithm includes: using a Gaussian filter to smooth the input image, using the Sobel operator to calculate the gradient amplitude image and angle image, applying non-maximum suppression to the gradient amplitude image, and using double threshold processing and connection analysis to detect and connect edges. The information that extracted by using Canny algorithm contains all the contour information in the picture, so it is necessary to distinguish each closed contour and save its information in the form of an array. A typical meniscus is shown in Fig. 2(e), where 'L' represents the length of the liquid meniscus in the axial direction, as is marked in the figure. Meniscus length is an important measure of the meniscus deformation process, and will be displayed in the following section.

The **waist** of the meniscus (w) is measured versus vertical distance from the nozzle edge (z), also shown in Fig. 2(e). Both w and z are measured in numbers of pixels. Therefore, the volume of the PCL melt at the nozzle is calculated via equation.

$$V = \sum_z \left(\frac{w(z) \times p_1}{2} \right)^2 \times \pi \times p_1 \quad (1)$$

The actual size (p_1) corresponding to one pixel can be obtained based on that the outer diameter of the nozzle is 1.26mm.

3. Results and discussion

3.1 Experimental conditions

As mentioned earlier, PCL is selected as the printing material. The PCL has a melting point of 60°C. Although it is difficult to measure the temperature of the nozzle tip, the temperature of the melting chamber is monitored and kept at $T_m=110^\circ\text{C}$. The viscosity of PCL at this temperature is estimated as $500 \text{ Pa}\cdot\text{s}^{20}$. The temperature of the underlying metal substrate is 135°C. As just mentioned, the flow of PCL melt is mainly due to the Poiseuille flow under the hydrostatic pressure, without intentional feeding. The nozzle length is about 6.5mm, the inner diameter is 0.86mm, and the height of the PCL melt above the needle is about 25mm. From this, it is estimated that the hydrostatic pressure is $\Delta P = 270\text{Pa}$. From Poiseuille's law ($Q = \frac{\pi \times r^4 \times \Delta P}{8\eta L}$), it can be estimated that the flow rate is 1.1nL/s. Although not shown here, the flow rate without applying electric voltage is measured to be 0.95nL/s, consistent with the above estimate. At the end of this article, it is also shown the electric stress has negligible effect on the flow rate.

During this experiment, the nozzle-substrate distance is kept constantly at 2mm. When the PCL melt at the nozzle reaches pre-set volume V_i , a high voltage of 2.7kV is applied. The rate of voltage ramping is 180V/s. Electric discharge may

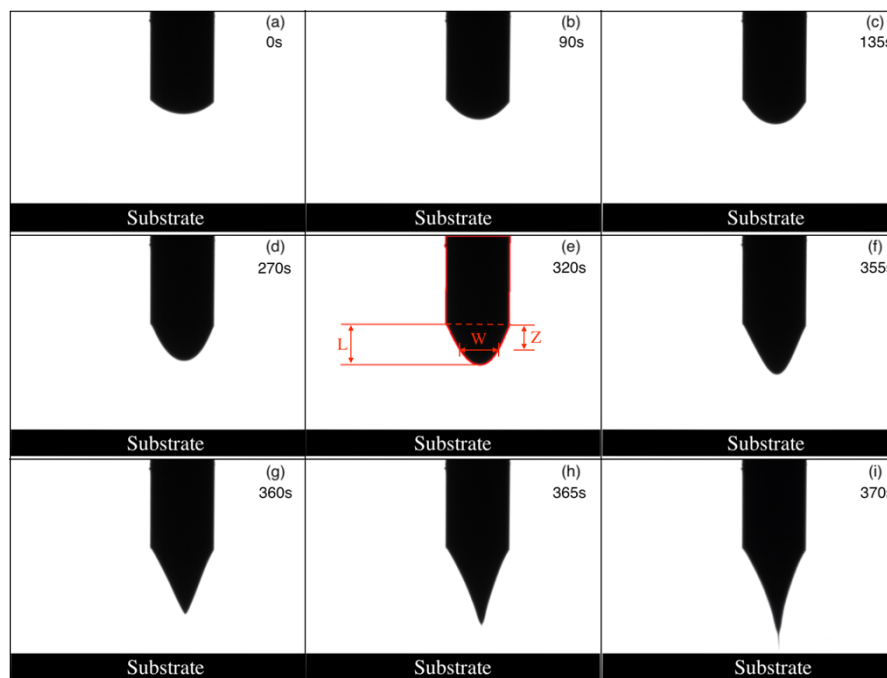


Fig. 2 The process of the meniscus deformation. The 2.7kV high voltage is applied to the nozzle when the volume of PCL melt at the nozzle is 185nL.

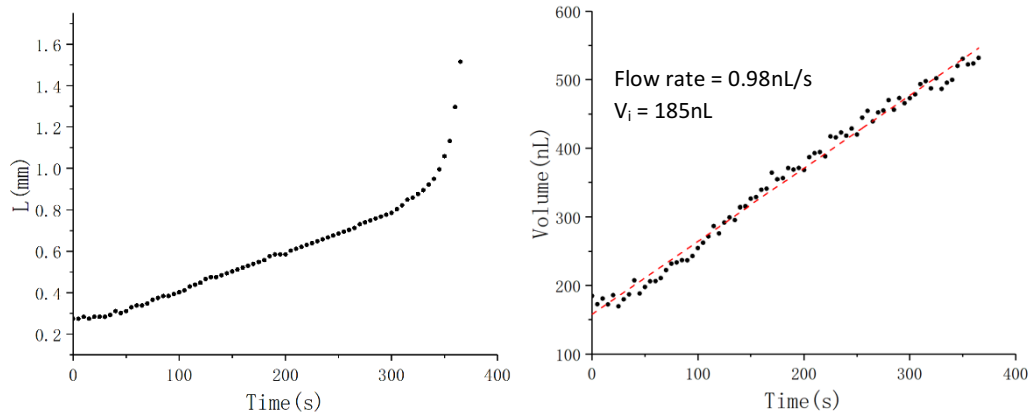


Fig. 3 (a) Meniscus length in the axial direction as a function of time, and (b) volume of PCL melt at the nozzle versus time. The 2.7kV high voltage is applied to the nozzle when the volume of PCL melt is 185nL. The flow rate is 0.98nL/s, estimated from the linear fitting.

occur in the process of forming the Taylor cone when a voltage higher than 2.7kV is applied.

3.2 Effects of initial volume V_i on meniscus deformation

Meniscus deformation processes have been studies for more than 50 initial volumes, ranging from 60nL to 800nL. Setting a sufficiently small initial volume, $V_i = 185$ nL to be more specific, Fig. 2 shows the process of meniscus deformation until the melt touches the substrate. As shown in Fig. 3(a), before $t=280$ s, the length of the meniscus increases linearly with time. At around $t=355$ s, the meniscus deforms into a cone with slight rounded tip (the Taylor cone). At this time, the liquid volume at the nozzle is 530nL. We will get back to this point later in the discussion. At around $t=370$ s, a fine jet emerges and finally reaches the substrate. The jet is much thinner than the

diameter of the nozzle. The volume of fluid at the nozzle increases linearly over time, as shown in Fig. 3(b). The flow rate is estimated to be 0.98nL/s. In our experimental setup, for initial volume less than about 270nL, meniscus deformation similar to that shown in Fig. 2 and 3 would occur, and a fine jet is generated. This start-up state, referred as state A, is clearly what we want. It may be beneficial for the writing process to maintain the high-resolution if we start moving the x-y stage as the jet touches the substrate.

Figure 4 shows complete process of liquid deformation in a similar experiment, but with the voltage ramped up at a rather large initial volume $V_i=749$ nL. The meniscus length L is shown in Fig. 5(a). Between 0s and 60s, L increases almost linearly versus time. Then L increases sharply, till around $t=115$ s, at which the meniscus exhibits the sharpest end tip, see Fig. 4(h). After that, the tip of the meniscus becomes more round in

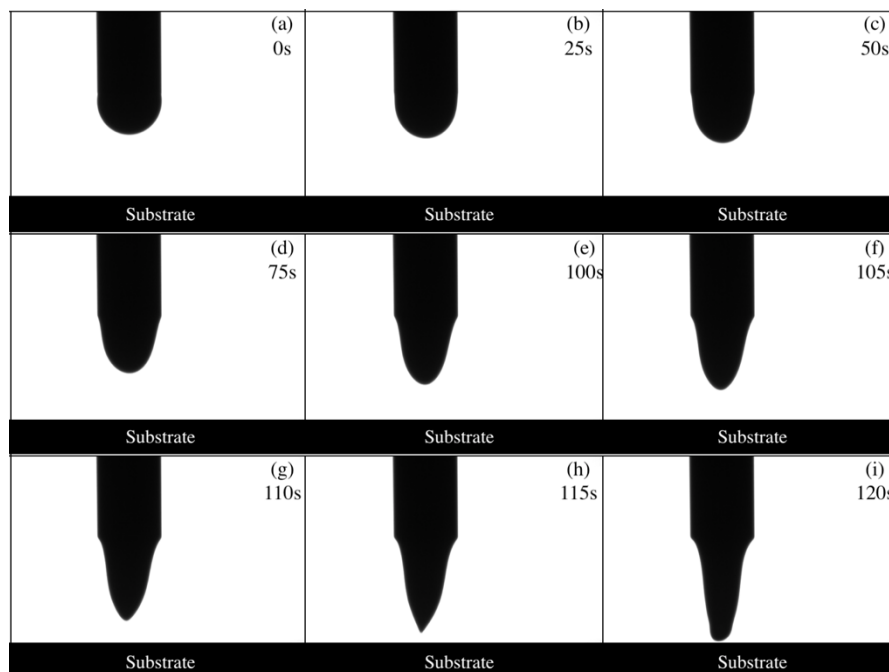


Fig. 4 The process of the meniscus deformation. The 2.7 (kV) high voltage is applied to the nozzle when the volume of PCL melt is 749nL.

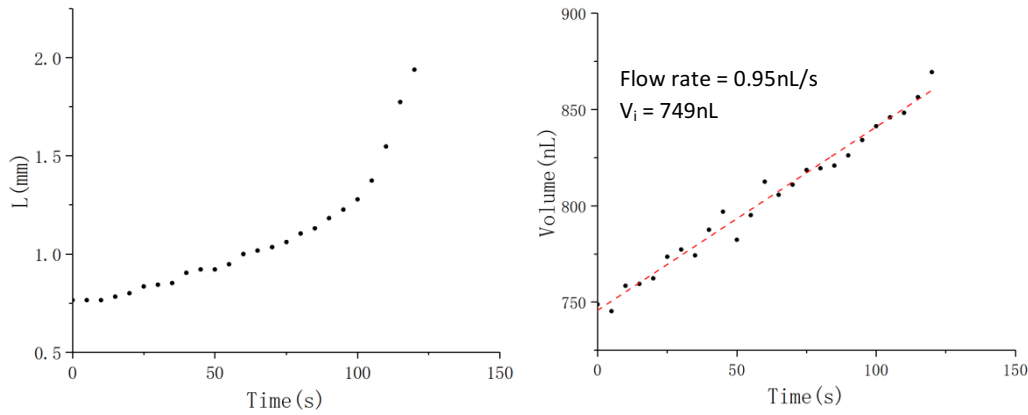


Fig. 5 (a) Meniscus length in the axial direction as a function of time, and (b) volume of PCL melt at the nozzle versus time. The 2.7kV high voltage is applied to the nozzle when the volume of PCL melt is 749nL. The flow rate is estimated from the linear fitting to be 0.95nL/s.

shape. Meanwhile, the waist of the meniscus gets narrower. Finally, the liquid contacts the substrate, with a large lump of liquid deposited. As can be seen from Fig. 5(b), the liquid volume has been increasing linearly throughout the process. The flow rate is consistent with what is expected from the Poiseuille flow. By ramping voltage at sufficiently large initial volume V_i (approximately greater than 500nL in this experimental setup), meniscus deformation process similar to that shown in Fig. 4 and 5 is prone to occur. Although not shown here, sometimes, the increase of the meniscus length slows down again, just before touching the substrate. This start-up state is referred as state B. Instead of a fine jet, this start-up state will cause a large lump of liquid delivered at the beginning of the printing.

By ramping voltage at an intermediate initial volume V_i (approximately 340-450nL in this experiment setup), start-up state C may appear. Figure 6 shows the deformation process of

the meniscus for an initial volume $V_i = 360\text{nL}$. And the meniscus length L versus time is plotted in Fig. 7(a). Before 160s, L increases slowly and linearly. And then L increases sharply with time. These behaviours are similar to those shown in Figs. 4 and 6. As shown in Figure 6(e), around $t=220\text{s}$, the Taylor cone similar to that in Fig. 2(f) is formed, the liquid volume is again 530nL. At $t=230\text{s}$, L reaches a maximum. Then, L gradually decreases, as clearly suggested in Fig. 7(a). It is worth noting that although L is decreasing, the total fluid volume is still increasing linearly, shown in Fig. 7(b). Although not shown here, it is confirmed the electric stress can drastically change the meniscus shape, the change of volume at the nozzle is basically determined by the Poiseuille's law and the hydrostatic pressure. Around $t=265\text{s}$, the meniscus length reaches a minimum. Later on, the meniscus will continue to elongate and finally contacts the substrate, due to continuous feeding of liquid, and also to

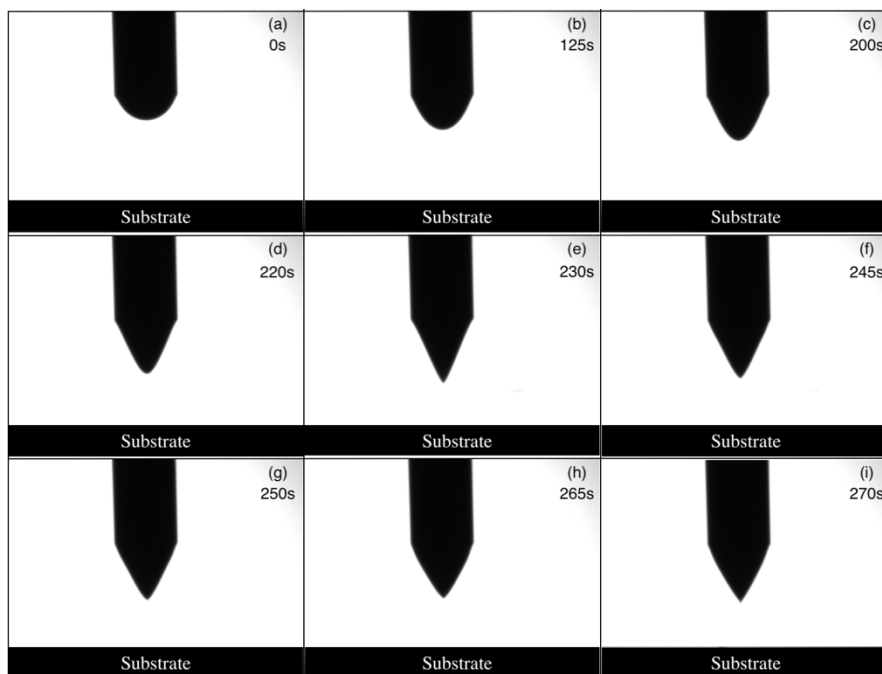


Fig. 6 The process of the meniscus deformation. 2.7kV high voltage is applied to the nozzle when the volume of PCL melt is 360nL

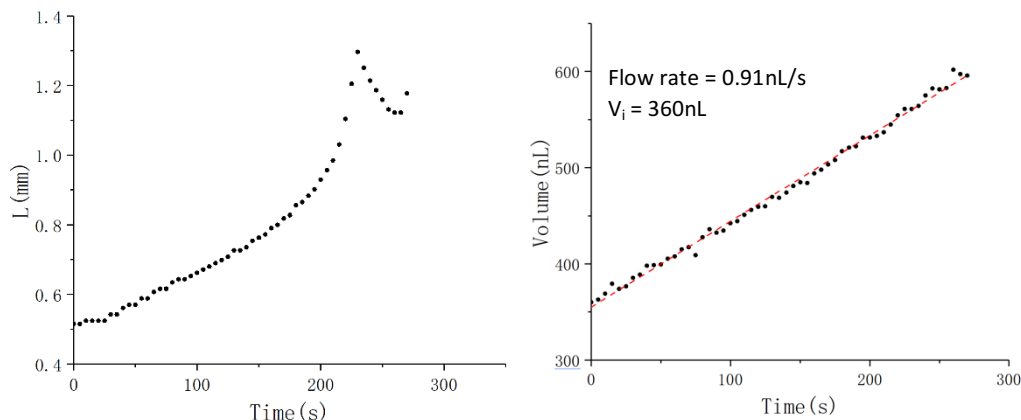


Fig. 7(a) Meniscus length in the axial direction as a function of time, and (b) volume of PCL melt at the nozzle versus time. The high voltage of 2.7kV is applied to the nozzle when the volume of PCL melt is 360nL. The flow rate is 0.91nL/s, also estimated from the linear fitting.

the electric stress. Two behaviors have been observed in the experiment: a fine jet may emerge, similar to what happened in Fig. 2; or a lump of liquid may finally contact the substrate, similar to that in Fig. 4. It is worth noting that the boundary between states A and C is not well defined. Specifically, for V_i in the range of 270 - 340nL, both states have a certain probability to appear.

As interpretations of the experimental results, we first explain why state B is more likely to show up with voltage applied at large initial volume V_i . According to Taylor's theory, the half angle of Taylor cone is about 49 degrees⁷. Some studies have shown that this half angle may be as small as 33 degrees²¹. This is more consistent with the Taylor cone observed in our experiment. At this condition, the volume of the Taylor cone is about 530nL (see Fig. 2(f) and Fig. 6(d)). If V_i is larger than this volume, the liquid cannot be deformed into the Taylor cone, and it is impossible to produce a fine jet. This is well

consistent with the boundary between state B and C. For state C, the stagnation or even the slight retraction of meniscus may be understood as precursor of shaking of the meniscus. Meniscus shaking is observed for ordinary dripping from a nozzle²². A lump of liquid, free-standing or attached to a nozzle, can also shake within a strong electric field, without any liquid emission^{23, 24}. For low viscosity fluids, the shaking amplitude is rather large²⁵. Due to the high viscosity of the PCL melt, the shaking cannot be observed as it damps out. That ramping voltage at sufficiently small liquid volume tends to give state A is not straightforward. Here, a plausible explanation is presented. In our experimental setup, the ambient temperature between the nozzle and substrate is about 50-60°C, which is much lower than the nozzle temperature at 110°C. The PCL melt cools down as it is extruded from the nozzle. Due to poor heat conduction of PCL, the time for temperature to reach equilibrium is rather long. The time constant is estimated as

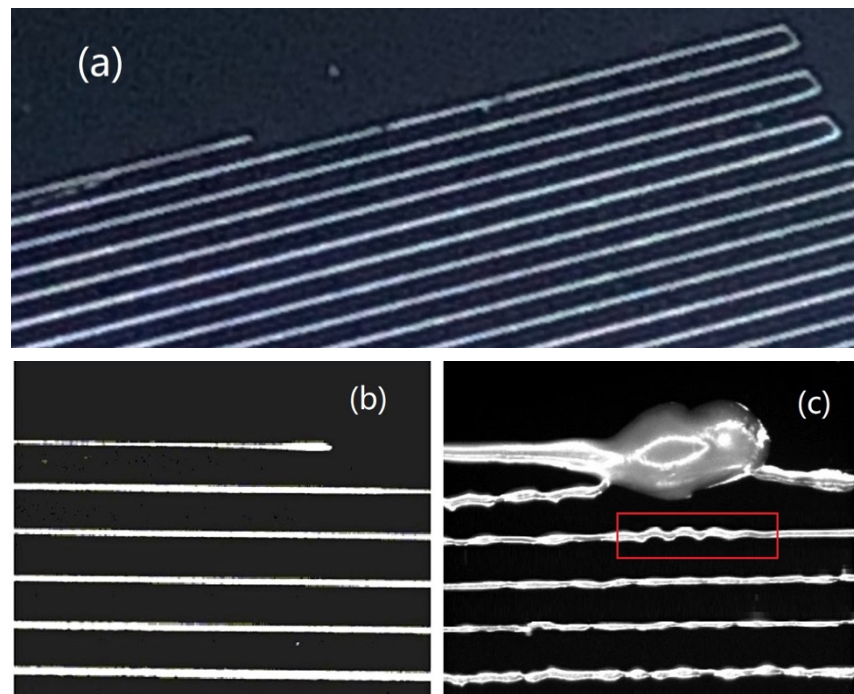


Fig. 8 The printing of a meander pattern. The printing begins as long as the liquid touches the substrate, with plotting speed 0.6mm/s. For (a) and (b), nozzle voltage is applied when PCL melt volume V_i is 182nL. For (c), V_i is 514nL.

$\left(\frac{C_p \rho}{\sigma}\right) L^2 = 15s$ ²⁶ where heat capacity is $C_p = 2 \times 10^3 \text{ J} \cdot \text{kg}^{-1} \text{K}^{-1}$ ²⁷, density is $\rho = 1.2 \times 10^3 \text{ kg} \cdot \text{m}^{-3}$, thermal conductivity is $\sigma = 0.16 \text{ W} \cdot \text{m}^{-1} \text{K}^{-1}$ ²⁸, meniscus length is taken to be $L = 1 \text{ mm}$. For smaller initial volume V_i , the whole process takes longer time and the liquid tends to stabilize at lower temperature. This leads to larger viscosity for the liquid, and therefore stronger suppression effect to the liquid shaking behaviour.

Based on the results in this section, to obtain high printing resolution, the liquid meniscus should make its contact with the substrate in the form of fine jet. For demonstration, a meander pattern is printed. The inter-line spacing is 0.3mm. Therefore, the voltage should be applied when the volume at the nozzle is sufficiently small. Specifically, $V_i = 182 \text{ nL}$. The Taylor cone is formed and a fine jet stream is generated. When the meniscus contacts the substrate, the platform begins to move at a speed (plotting speed) of 0.6mm/s, and with an acceleration of 3.75mm/s². A pattern with consistent line width is realized, as shown in Fig. 8(a). And Fig. 8(b) shows the starting position in more detail. The start of the scribed line is very thin and this is exactly what we expect for higher resolution printing. As a control experiment, voltage is not applied until the liquid volume at the nozzle is large enough. Specifically, $V_i = 514 \text{ nL}$. The meniscus contacts with the substrate, with a large lump of liquid deposited, shown in Fig. 8(c). In some previous literatures, there was a drop of liquid at the start position of the printing, likely of the same origin. This large liquid drop seriously interferes with subsequent printing. Specifically, the adjacent line moves towards and finally touches the large liquid drop at the start point. For the third line, a behaviour known as fibre pulsing²⁹ is observed, marked by the red rectangle. Fibre pulsing is due to mismatch between the jetting speed and the plotting speed. However, we are not sure whether the fibre pulsing here is directly caused by the large liquid drop at the starting point.

4. Conclusions

Experiments are performed to improve the resolution at the start-up stage of the direct writing, by using a home build E-FDM system. The melted PCL is chosen as printing material. The nozzle is fixed 2mm above the substrate. The temperatures of the nozzle and the substrate are held steady. At a set of initial volume V_i , 2.7kV voltage is applied to the nozzle, at fixed ramping rate. It is found that three deformation processes can appear, leading to different contacting behaviours with the substrate. When V_i is sufficiently small (less than about 270nL in this experiment), A fine jet with diameter much smaller than the nozzle appears. When V_i is sufficiently large, the liquid makes the contact with the substrate in a spindle shape, and with a large lump of liquid delivered. For V_i in the middle range, the deformation of meniscus tends to produce jet, but it fails. The length of meniscus decreases slightly after reaching the maximum. Possible interpretations of the experimental results are given. Obviously in actual application, for better printing resolution at the start position, ramping voltage at sufficiently small liquid volume V_i is suggested.

Conflicts of interest

There are no conflicts to declare.

Notes and references

1. K. S. Boparai, R. Singh and H. Singh, *Rapid Prototyping Journal*, 2016, **22**, 281-299.
2. I. Matai, G. Kaur, A. Seyedsalehi, A. McClinton and C. T. Laurencin, *Biomaterials*, 2020, **226**, 119536.
3. E. Mathew, G. Pitzanti, E. Larraneta and D. A. Lamprou, *Pharmaceutics*, 2020, **12**.
4. G. Gaal, M. Mendes, T. P. de Almeida, M. H. O. Piazzetta, Å. L. Gobbi, A. Riul and V. Rodrigues, *Sensors and Actuators B: Chemical*, 2017, **242**, 35-40.
5. M. D. Monzón, I. Gibson, A. N. Benítez, L. Lorenzo, P. M. Hernández and M. D. Marrero, *The International Journal of Advanced Manufacturing Technology*, 2013, **67**, 2717-2726.
6. M. S. Onses, E. Sutanto, P. M. Ferreira, A. G. Alleyne and J. A. Rogers, *Small*, 2015, **11**, 4237-4266.
7. G. Taylor, *Proceedings of the Royal Society A: Mathematical, Physical and Engineering Sciences*, July 28 1964, **280**, 383-397.
8. D. Li and Y. Xia, *Advanced Materials*, 2004, **16**, 1151-1170.
9. A. Haider, S. Haider and I.-K. Kang, *Arabian Journal of Chemistry*, 2018, **11**, 1165-1188.
10. T. Kong, H. A. Stone, L. Wang and H. C. Shum, *Proceedings of the National Academy of Sciences*, 2018, **115**, 6159-6164.
11. T. D. Brown, P. D. Dalton and D. W. Hutmacher, *Progress in Polymer Science*, 2016, **56**, 116-166.
12. T. M. Robinson, D. W. Hutmacher and P. D. Dalton, *Advanced Functional Materials*, 2019, **29**.
13. B. Zhang, B. Seong, V. Nguyen and D. Byun, *Journal of Micromechanics and Microengineering*, 2016, **26**.
14. C. Wei and J. Dong, *Journal of Manufacturing Processes*, 2014, **16**, 257-263.
15. Q. Chen, X. Mei, Z. Shen, D. Wu, Y. Zhao, L. Wang, X. Chen, G. He, Z. Yu, K. Fang and D. Sun, *Opt Lett*, 2017, **42**, 5106-5109.
16. X. Yu, M. Feng, R. Zhang, Y. Feng, H. You, F. Guo, S. Chen and D. Zhang, *Organic Electronics*, 2017, **51**, 442-445.
17. S. Y. Min, T. S. Kim, B. J. Kim, H. Cho, Y. Y. Noh, H. Yang, J. H. Cho and T. W. Lee, *Nat Commun*, 2013, **4**, 1773.
18. M. A. Woodruff and D. W. Hutmacher, *Progress in Polymer Science*, 2010, **35**, 1217-1256.
19. H. Lian and Z. Meng, *Mater Sci Eng C Mater Biol Appl*, 2017, **74**, 117-123.
20. V. Speranza, A. Sorrentino, F. De Santis and R. Pantani, *ScientificWorldJournal*, 2014, **2014**, 720157.
21. A. L. Yarin, S. Koombhongse and D. H. Reneker, *Journal of Applied Physics*, 2001, **90**, 4836-4846.
22. C. Clanet and J. C. Lasheras, *Journal of Fluid Mechanics*, 1999, **383**, 307-326.
23. H. Sato, N. Kaji, T. Mochizuki and Y. H. Mori, *Physics of Fluids*, 2006, **18**.
24. A. J. Hijano, I. G. Loscertales, S. E. Ibanez and F. J. Higuera, *Phys Rev E Stat Nonlin Soft Matter Phys*, 2015, **91**, 013011.

ARTICLE

Journal Name

25.	H. Zhang, C. Wang, R. Jia, F. Wang, Y. Wang, Z. Wang, X. Chen, X. Wang and J. Gui, <i>Biomed Microdevices</i> , 2019, 21 , 64.	28.	O. J. Botlhoko, J. Ramontja and S. S. Ray, <i>RSC Advances</i> , 2017, 7 , 33751-33756.
26.	R. Reif, <i>Fundamentals of Statistical and Thermal Physics</i> , 2009.	29.	G. Hochleitner, A. Youssef, A. Hrynevich, J. N. Haigh, T. Jungst, J. Groll and P. D. Dalton, <i>BioNanoMaterials</i> , 2016, 17 .
27.	D. Liu and C. Zhong, <i>Polymer Journal</i> , 2002, 34 , 954-961.		